Analysis and Modeling of a Voltage Doubler Rectifier Fed by a Piezoelectric Transformer

Gregory Ivensky, Moshe Shvartsas, and Shmuel (Sam) Ben-Yaakov, *Member, IEEE*

***Abstract*—Piezoelectric transformers (PZT) can be used advantageously in high output voltage dc–dc converters. In such applications the output section includes a voltage doubling rectification scheme to help increase the output voltage. This topology was modeled and analyzed by considering the expected voltage and current waveforms under the first harmonics approximation. The results were then used to build a linear ac equivalent circuit that emulates the ac–dc stage. The proposed model was verified against simulation and experimental results.**

***Index Terms*—High voltage, modeling, piezoelectric transformers, voltage doubler.**

I. Introduction

PIEZOELECTRIC transformers (PZT) were shown to be advantageous in dc–dc converter applications and in cold cathode fluorescent lamps drivers [1]–[13]. The favorable attributes of the PZT are low weight and size and potentially low cost. The latter is particularly true for single layer PZTs, as the one used in this investigation, that are made of a polarized piece of piezoelectric material on which the electrodes are deposited. The present (mid 2003) price of PZT devices is relatively high due to the fact that they are not manufactured in high volume. One additional important characteristic is the high voltage isolation of the ceramic materials used to build PZTs. This advantage is especially beneficial when the PZT is applied in high output voltage (HV) applications. In these cases, the inherent high voltage isolation eliminates the relatively larger size and higher production costs normally associated with high voltage electromagnetic transformers. Potential applications of PZT based HV converters include ionizers, ion generators, electron microscope, photomultiplier power supplies and others.

In HV converters, one would like to avoid the use of output filter inductors that becomes bulky and highly expensive under the HV operating conditions. The conventional alternative is the capacitor filter that is more practical under high output voltage—and hence relatively lower current—conditions. Considering the primary objective of obtaining a high output voltage, a voltage doubler rectifier will be the preferred choice. The simplest voltage doubler rectifier has a nonsymmetrical half-wave topology with one capacitor C and two diodes (Fig. 1) [11]–[13]. It has been documented that in this operating scheme the output voltages of PZT and of the rectifier and the resonant frequency of the PZT are highly dependent on the load resistance $\mathrm{R_L}$, but no systematic analysis has been presented hitherto to examine these relationships.

In this study we develop a model of the voltage doubler rectifier in the case when the rectifier is fed by a circuit with a high quality factor (Q). We apply this model together with the equivalent circuit of the PZT to derive a common ac equivalent circuit that emulates the behavior of the PZT based HV ac–dc stage. We then obtain analytical expressions describing the interdependence of key parameters.

II. Diodes' Conduction Angle

The conventional equivalent circuit of the PZT includes (Fig. 2): an ideal transformer with turn ratio n, an input capacitor $\mathrm{C_{in}}$, an output capacitor $\mathrm{C_o}$ and a series branch $\mathrm{R_mL_rC_r}$ which represents mechanical resonance at the frequency

$$\mathrm{f_r} = \frac{1}{2\pi\sqrt{\mathrm{L_rC_r}}} \tag{1}$$

and losses (emulated by mechanical equivalent resistance $\mathrm{R_m}$).

In this model, the action of the ideal transformer is represented by two dependent sources: a voltage source at the primary and a current source at the secondary [14]. The turns ratio appears as the gain factor of these sources. The primary and secondary dc components are blocked by $\mathrm{C_r}$—as is in the case of the physical PZT.

In typical HV ac–dc application, the PZT will be fed by an ac signal. Different inverter topologies can be used at the input side but considering the high Q of the PZT device and the fact that operation is normally near the resonant frequency, only the first harmonics of the input voltage will affect the resonant current.

Simulated current and voltage waveforms of the rectifier (Fig. 1), connected to the output of PZT (Fig. 2), are shown in Fig. 3. The angle $\vartheta = 2\pi\mathrm{ft}$ is normalized time in radians, f is the switching frequency and t is time. Analysis (and simulation) is carried out under the following basic assumptions.

1) Diodes, inductor and capacitors are ideal.
2) The mechanical equivalent resistance $\mathrm{R_m}$ is much lower than the characteristic impedance $\sqrt{\mathrm{L_r/C_r}}$ of the $\mathrm{R_mL_rC_r}$ branch (Fig. 2) and hence the current $\mathrm{i_r}$ of this branch can be approximated by a sinusoidal waveform:

$$\mathrm{i_r} = \mathrm{I_{rm}}\sin\vartheta \tag{2}$$

where $\mathrm{I_{rm}}$ is the peak of this current.
3) The time constant $\mathrm{R_LC}$ (Fig. 1) is much larger than the switching period 1/f and therefore the ripple of the load voltage $\mathrm{V_L}$ can be neglected.

Manuscript received January 28, 2003; revised August 21, 2003. This work was supported by Israel Science Foundation Grant 113/02-1. Recommended by Associate Editor R.-L. Lin.

The authors are with the Power Electronics Laboratory, Department of Electrical and Computer Engineering, Ben-Gurion University of the Negev, Beer-Sheva 84105, Israel (e-mail: sby@ee.bgu.ac.il).

Digital Object Identifier 10.1109/TPEL.2003.823179

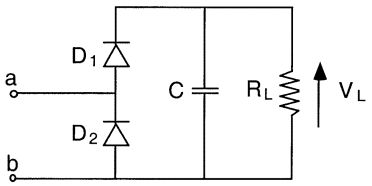

Fig. 1. Non-symmetrical topology of a voltage-doubler rectifier.

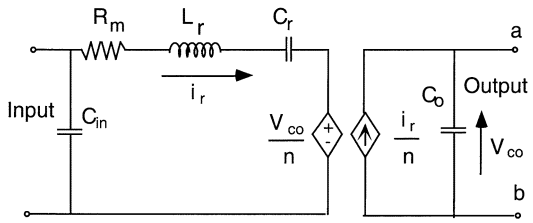

Fig. 2. Equivalent circuit of a piezoelectric transformer (PZT).

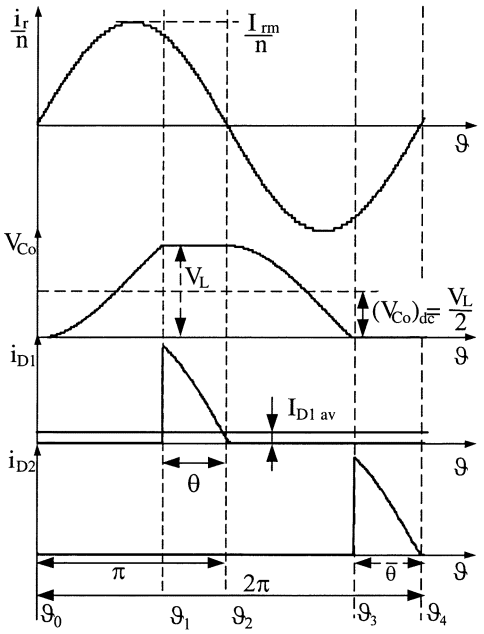

Fig. 3. Simulated current and voltage waveforms of the voltage doubler rectifier (Fig. 1) fed by a piezoelectric transformer (Fig. 2).

Referring to Figs. 1–3, the reflected current $\mathrm{i_r}/\mathrm{n}$ flows through the capacitor $\mathrm{C_o}$ of PZT during the nonconduction intervals of both diodes ($\vartheta_0\vartheta_1$ and $\vartheta_2\vartheta_3$) and through the diodes $\mathrm{D_1}$ or $\mathrm{D_2}$ during their conduction intervals ($\vartheta_1\vartheta_2$ and $\vartheta_3\vartheta_4$). Duration of these conduction intervals is defined as θ. The voltage across the capacitor $\mathrm{C_o}$ ($\mathrm{v_{Co}}$) is equal to the load voltage $\mathrm{V_L}$ during the conduction interval of $\mathrm{D_1}$ (interval $\vartheta_1\vartheta_2$) and is zero during the conduction interval of $\mathrm{D_2}$ (interval $\vartheta_3\vartheta_4$).

The voltage $\mathrm{v_{Co}}$ during the nonconduction intervals of both diodes ($\mathrm{D_1}$, $\mathrm{D_2}$) can be divided into distinct operational segments by applying the following initial conditions (Figs. 1–3):

at $\vartheta_0 = 0$ the current $\mathrm{i_r}/\mathrm{n}$ (2) changes its direction and therefore the diode $\mathrm{D_2}$ ceases to conduct, $\mathrm{v_{Co}} = 0$;
at $\vartheta_1 = \pi - \theta$ the capacitor's voltage $\mathrm{v_{Co}}$ reaches the load voltage $\mathrm{V_L}$ and therefore the diode $\mathrm{D_1}$ begins to conduct;
at $\vartheta_2 = \pi$ the current $\mathrm{i_r}/\mathrm{n}$ (2) changes its direction and therefore the diode $\mathrm{D_1}$ ceases to conduct, $\mathrm{v_{Co}} = \mathrm{V_L}$;
at $\vartheta_3 = 2\pi - \theta$ the capacitor's voltage $\mathrm{v_{Co}}$ reaches zero and therefore the diode $\mathrm{D_2}$ begins to conduct.

Applying (2) along with the above boundary conditions we get for the interval $\vartheta_0\vartheta_1$

$$\mathrm{v_{Co}} = \frac{\mathrm{V_L}}{1+\cos\theta}(1-\cos\vartheta) \tag{3}$$

and for the interval $\vartheta_2\vartheta_3$

$$\mathrm{v_{Co}} = \frac{\mathrm{V_L}}{1+\cos\theta}(\cos\theta-\cos\vartheta). \tag{4}$$

Taking into account that $\mathrm{v_{Co}} = \mathrm{V_L}$ or $\mathrm{v_{Co}} = 0$ in the conducting intervals of the diodes and applying (3) and (4) we obtain the dc component of voltage $\mathrm{v_{Co}}$ during the switching period $\vartheta_0\vartheta_4$

$$(\mathrm{V_{Co}})_{\mathrm{dc}} = \frac{\mathrm{V_L}}{2}. \tag{5}$$

Note that the dc component of $\mathrm{v_{Co}}$ is blocked by the ceramic material of the PZT. This galvanic isolation effect is emulated by $\mathrm{C_r}$ in the equivalent circuit presentation (Fig. 2).

The same value has the peak of the ac component of the capacitor's $\mathrm{C_o}$ voltage

$$(\mathrm{V_{Co}})_{\mathrm{ac\ pk}} = \frac{\mathrm{V_L}}{2}. \tag{6}$$

Hence, the output voltage of the rectifier V_L is twice higher than the peak of the ac component of the capacitor's $\mathrm{C_o}$ voltage that can be considered as the input voltage of the rectifier. Therefore this type of rectifier operates as a voltage doubler.

The peak of the reflected current of the $\mathrm{R_mL_rC_r}$ branch of the PZT-model (Fig. 2) is found from (2) and (3) or (4)

$$\frac{\mathrm{I_{rm}}}{\mathrm{n}} = \frac{\mathrm{V_L}\omega\mathrm{C_o}}{1+\cos\theta} \tag{7}$$

where $\omega = 2\pi\mathrm{f}$.

The current of the load $\mathrm{I_L}$ is equal to the average current of the diode $\mathrm{D_1}$

$$\mathrm{I_L} = \mathrm{I_{D1av}} = \frac{1}{2\pi}\int_{\pi-\theta}^{\pi}\frac{\mathrm{I_{rm}}}{\mathrm{n}}\sin\vartheta\mathrm{d}\vartheta = \frac{1}{2\pi}\frac{\mathrm{I_{rm}}}{\mathrm{n}}(1-\cos\theta) \tag{8}$$

or applying (7)

$$\mathrm{I_L} = \mathrm{I_{D1\ av}} = \frac{1}{2\pi}\mathrm{VL}\omega\mathrm{C_o}\tan^2\left(\frac{\theta}{2}\right). \tag{9}$$

On the other hand

$$\mathrm{I_L} = \mathrm{I_{D1\ av}} = \frac{\mathrm{V_L}}{\mathrm{R_L}}. \tag{10}$$

From (9) and (10) we obtain the diodes conduction angle

$$\theta = 2\tan^{-1}\sqrt{\frac{2\pi}{\omega\mathrm{C_oR_L}}}. \tag{11}$$

Relationship (11) is depicted in Fig. 4.

III. RC Equivalent Model of the Voltage Doubler Rectifier

Since the top and bottom of the capacitor's C_o voltage v_{Co} waveform are flat during the conducting intervals of the diodes (Fig. 3), the waveform of this voltage includes high harmonics. In contrast, the waveform of the current i_r of the branch $R_m L_r C_r$ is assumed to be practically a sine wave—due to the high Q of the circuit. Under these conditions only the fundamental harmonic of the voltage v_{Co} affects the output power

$$P_L = \frac{1}{2} V_{Co(1)m} \frac{I_{rm}}{n} \cos \varphi_{(1)} \tag{12}$$

where $V_{Co(1)m}$ is the peak of the fundamental harmonic of the voltage v_{Co} and $\varphi_{(1)}$ is its phase angle referred to the instant $\vartheta_0 = 0$. The values of $V_{Co(1)m}$ and $\varphi_{(1)}$ are found from

$$V_{Co(1)m} = k_{v(1)} (V_{Co})_{ac.pk} \tag{13}$$

$$\varphi_{(1)} = \tan^{-1} \left(\frac{a_{v(1)}}{b_{v(1)}} \right) \tag{14}$$

where $k_{v(1)}$ is the voltage waveform coefficient [15]

$$k_{v(1)} = \sqrt{a_{v(1)}^2 + b_{v(1)}^2} \tag{15}$$

and

$$a_{v(1)} = -\frac{2}{\pi} \left[\frac{\pi - \theta + \frac{1}{2} \sin(2\theta)}{1 + \cos \theta} \right] \tag{16}$$

$$b_{v(1)} = \frac{2}{\pi} (1 - \cos \theta). \tag{17}$$

Note that $\varphi_{(1)} < 0$ because $a_{v(1)} < 0$. Equations (13)–(17) show that $\varphi_{(1)}$ and $k_{v(1)}$ are uniquely defined by θ. Taking into account (11) we find that $\varphi_{(1)}$ and $k_{v(1)}$ are functions of $\omega C_o R_L$. These relationships are depicted in Fig. 4.

Considering the fact that $\varphi_{(1)} < 0$, the network including the capacitor C_o, output rectifier and load can be represented by a $R_{eq} C_{eq}$ parallel equivalent circuit [Fig. 5(a)]. The equivalent load resistance R_{eq} was found from

$$P_L = \frac{V_{Co(1)m}^2}{2R_{eq}} = \frac{V_L^2}{R_L}. \tag{18}$$

Applying (18), (13), and (6)

$$R_{eq} = \frac{k_{v(1)}^2 R_L}{8}. \tag{19}$$

The equivalent capacitance C_{eq} was found from Fig. 5(b) to be

$$C_{eq} = \frac{\tan |\varphi_{(1)}|}{\omega R_{eq}}. \tag{20}$$

Note that C_{eq} includes two components: the PZT output capacitance C_o and an additional capacitance C_{ad}

$$C_{eq} = C_o + C_{ad}. \tag{21}$$

From (19)–(21)

$$\frac{C_{ad}}{C_o} = \frac{8}{\omega C_o R_L} \frac{\tan |\varphi_{(1)}|}{k_{v(1)}^2} - 1. \tag{22}$$

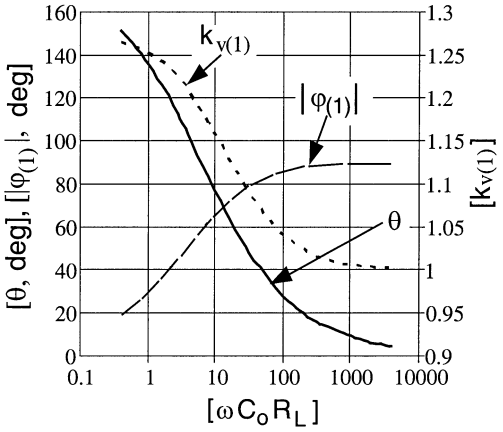

Fig. 4. Rectifier conduction angle θ, the phase angle $\varphi_{(1)}$ and the voltage waveform coefficient $k_{v(1)}$ as functions of the load coefficient $\omega C_o R_L$.

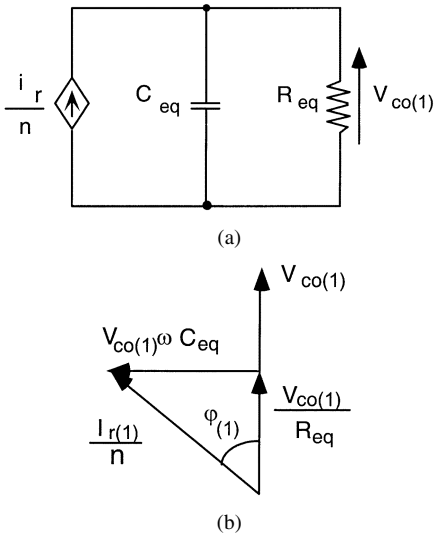

Fig. 5. Equivalent $R_{eq} C_{eq}$ circuit replacing the reflected rectifier-load network fed by the current (I_r/n): (a) topology and (b) vector diagram.

The relationships (R_{eq}/R_L) and (C_{ad}/C_o) as a function of $\omega C_o R_L$, calculated by (11), (14)–(17), (19), and (22) are depicted on Fig. 6. Note that (C_{ad}/C_o) is small when $\omega C_o R_L > 40$.

IV. Output Voltage of the Rectifier

Applying the equivalent resistance R_{eq} and the equivalent capacitance C_{eq}, the system including the PZT and the output rectifier can be represented by the equivalent circuit of Fig. 7. $V_{in(1)m}$ and $(V_{Co(1)m}/n)$ are the peaks of the first harmonic of the input and output voltages of the equivalent circuit (Fig. 7).

The expression of the (ac output)/(ac input) voltage ratio

$$k_{21} = \frac{V_{Co(1)m}}{n V_{in(1)m}} \tag{23}$$

can be found by analyzing this equivalent circuit [14] as (24), shown at the bottom of the next page, where $\omega_r = 2\pi f_r$.

In the case $\omega = \omega_r$ the impedance of the series circuit $L_r C_r$ is zero and therefore the AC input voltage is applied to the output parallel circuit $n^2 C_{eq} \| R_{eq}/n^2$ via the equivalent mechanical resistance R_m. That is why $k_{21} < 1$. In HV applications since R_m

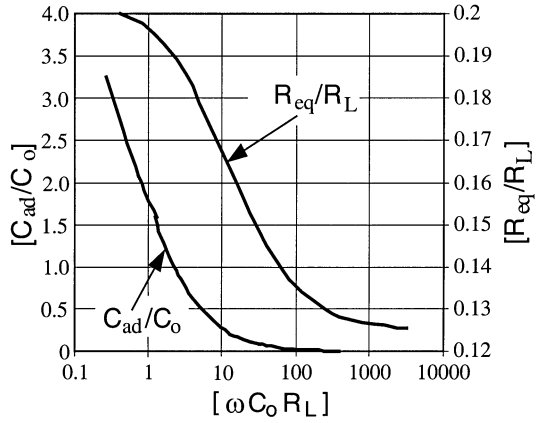

Fig. 6. Equivalent load resistance $\mathrm{R_{eq}(pu)}$ and apparent additional capacitance $\mathrm{C_{ad}(pu)}$ as functions of the load coefficient $\omega \mathrm{C_o R_L}$.

is much lower than the reflected impedance of the parallel circuit, $\mathrm{k_{21}}$ will be near unity when $\omega = \omega_\mathrm{r}$. The load voltage, denoted in this case as $(\mathrm{V_L})_{\mathrm{f_r}}$, can be obtained from (6), (13), and (23)

$$(\mathrm{V_L})_{\mathrm{f_r}} \approx \frac{2\mathrm{n}}{\mathrm{k_{v(1)}}} \mathrm{V_{in(1)m}}. \tag{25}$$

In the case $\omega > \omega_\mathrm{r}$ the series circuit $\mathrm{L_r C_r}$ is inductive and therefore the voltage across the parallel circuit $\mathrm{n^2 C_{eq} || R_{eq}/n^2}$ can be higher than the ac input voltage: $\mathrm{k_{21}} > 1$. The expression of the frequency ratio $\omega_\mathrm{m}^* = (\omega/\omega_\mathrm{r})_\mathrm{max}$ corresponding to the maximum value of $\mathrm{k_{21}}$ $((\mathrm{k_{21}})_\mathrm{max})$ was found from (24) under the assumption that the values $\varphi_{(1)}$ and $\mathrm{C_{eq}}$ are constant and independent of the frequency ratio $(\omega/\omega_\mathrm{r})$

$$\omega_\mathrm{m}^* = \left(\frac{\omega}{\omega_\mathrm{r}}\right)_\mathrm{max} = \sqrt{1 + \frac{\mathrm{C_r}}{\mathrm{n^2 C_{eq}}} \sin^2 \varphi_{(1)}}. \tag{26}$$

The above equation implies

$$\omega_\mathrm{m}^* = \sqrt{1 + \frac{\mathrm{C_r}}{\mathrm{n^2 C_o}} \frac{\mathrm{C_o}}{\mathrm{C_{eq}}} \sin^2 \varphi_{(1)}} < \sqrt{1 + \frac{\mathrm{C_r}}{\mathrm{n^2 C_o}}}. \tag{27}$$

Note that $\omega_\mathrm{r}\sqrt{1 + (\mathrm{C_r}/\mathrm{n^2 C_o})}$ is the resonant frequency of the equivalent circuit (Fig. 7) under no load condition $(\mathrm{R_{eq}} = \infty)$ and is therefore the highest resonant frequency of the circuit. On the other hand

$$\omega_\mathrm{m}^* > 1. \tag{28}$$

Hence

$$1 < \omega_\mathrm{m}^* < \sqrt{1 + \frac{\mathrm{C_r}}{\mathrm{n^2 C_o}}}. \tag{29}$$

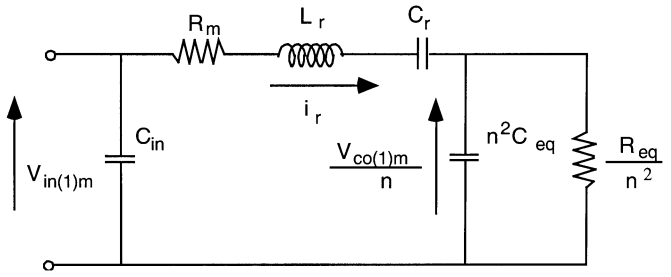

Fig. 7. AC equivalent circuit of the system: PZT, output rectifier and load.

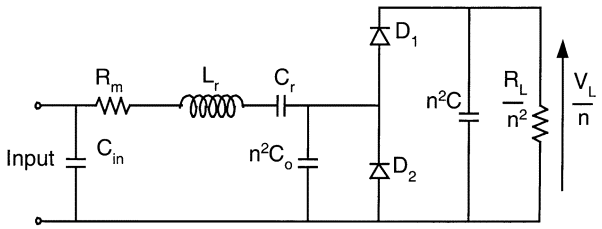

Fig. 8. AC/DC equivalent circuit of the system: PZT-voltage doubler rectifier.

Inserting in (29) the parameter values of the experimental PZT (as measured by our group) we obtain

$$1 < \omega_\mathrm{m}^* < 1.1. \tag{30}$$

Figs. 4 and 6 show that such a small frequency range causes insignificant changes in the values of $\varphi_{(1)}$ and $\mathrm{C_{ad}}$, which is the variable part of $\mathrm{C_{eq}}$ (21). Therefore our assumption about $\mathrm{C_{eq}}$ and $\varphi_{(1)}$ independence of the frequency ratio $(\omega/\omega_\mathrm{r})$ is a good approximation to obtain $(\omega/\omega_r)_\mathrm{max}$ from (26).

Inserting (26) into (24) we obtain the maximum value of $\mathrm{k_{21}}$ $((\mathrm{k_{21}})_\mathrm{max})$ [14]

$$(\mathrm{k_{21}})_\mathrm{max} = \frac{1}{\cos\varphi_{(1)} + \frac{\mathrm{n^2 R_m}}{\mathrm{R_{eq}}\cos\varphi_{(1)}}}. \tag{31}$$

The expression of the normalized maximum value of the load voltage (i.e. output voltage of the rectifier)

$$\mathrm{V_{L\,max}^*} = \frac{\mathrm{V_{L\,max}}}{\mathrm{V_{in(1)m}}} \tag{32}$$

is found from (6), (13), (23), and (31) under the assumption that $\mathrm{k_{v(1)}}$ and $\varphi_{(1)}$ are independent of $(\omega/\omega_\mathrm{r})$

$$\mathrm{V_{L\,max}^*} = \frac{2\mathrm{n}(\mathrm{k_{21}})_\mathrm{max}}{\mathrm{k_{v(1)}}} = \frac{2\mathrm{n}}{\mathrm{k_{v(1)}}\left[\cos\varphi_{(1)} + \frac{\mathrm{n^2 R_m}}{\mathrm{R_{eq}}\cos\varphi_{(1)}}\right]}. \tag{33}$$

This equation can be simplified if $\mathrm{R_m}$ can be neglected

$$\mathrm{V_{L\,max}^*} = \frac{2\mathrm{n}}{\mathrm{k_{v(1)}}\cos\varphi_{(1)}}. \tag{34}$$

$$\mathrm{k_{21}} = \frac{1}{\sqrt{\left\{1 - \frac{\mathrm{n^2 C_{eq}}}{\mathrm{C_r}}\left[\left(\frac{\omega}{\omega_\mathrm{r}}\right)^2 - 1\right] + \frac{\mathrm{n^2 R_m}}{\mathrm{R_{eq}}}\right\}^2 + \left\{\frac{\mathrm{n^2}}{\omega \mathrm{C_r R_{eq}}}\left[\left(\frac{\omega}{\omega_r}\right)^2 - 1\right] + \mathrm{n^2}\omega \mathrm{C_{eq} R_m}\right\}^2}} \tag{24}$$

TABLE I
MAXIMUM LOAD VOLTAGE AS A FUNCTION OF LOAD RESISTANCE R_L AT OPTIMAL OPERATING FREQUENCY. SIMULATION AND THEORETICAL RESULTS. SUBSCRIPT $_{mod.ac}$ DENOTES SIMULATION RESULTS OF THE AC MODEL (FIG. 7). SUBSCRIPT $_{c-b-c}$ DENOTES RESULTS OF CYCLE-BY-CYCLE SIMULATION OF THE AC/DC CIRCUIT (FIG. 8). SUBSCRIPT $_{anal}$ DENOTES ANALYTICAL VALUES, ACCORDING TO THE EQUATIONS DEVELOPED IN THIS STUDY

R_L	R_{eq}	C_{eq}	$(k_{21})_{max}$	$f_{m.mod.ac}$	$\omega^*_{m.mod.ac}$	$V^*_{Lmax.mod.ac}$	$V^*_{Lmax.c-b-c}$	$\omega^*_{m.c-b-c}$	$V^*_{Lmax.anal}$	$\omega^*_{m.anal}$
kOhm	Ohm	nF	-	Hz	-	-	-	-	-	-
1	200	2.410	0.6645	100860	1.0003	1.050	1.054	1.0001	1.050	1.0003
2	397	1.740	0.8296	100900	1.0007	1.316			1.317	1.0007
5	964	1.160	1.0542	101051	1.0022	1.700			1.697	1.0022
10	1850	0.892	1.2973	101279	1.0045	2.130	2.114	1.0040	2.126	1.0044
20	3500	0.720	1.7119	101592	1.0076	2.892			2.879	1.0075
50	7960	0.596	2.8172	101976	1.0114	4.993			4.955	1.0113
100	14800	0.550	4.4272	102156	1.0132	8.139	8.116	1.0128	8.071	1.0131
200	27900	0.527	7.0821	102246	1.0140	13.420			13.329	1.0141
500	66000	0.515	12.417	102294	1.0145	24.170			24.122	1.0145
1000	129000	0.512	17.170	102301	1.0146	33.825	33.740	1.0142	33.971	1.0146
2000	254000	0.511	21.504	102312	1.0147	42.658			42.996	1.0147
5000	629000	0.510	25.451	102312	1.0147	50.730	50.460	1.0143	51.295	1.0147

V. SIMULATION AND EXPERIMENTAL RESULTS

The validation of the proposed approach was confirmed by simulation and experiments. Simulation was carried out in two ways.

1) By running a time domain simulation on the complete nonlinear circuit, i.e., the original PZT model and rectifier (Fig. 8). In the following this simulation is referred to as "cycle- by- cycle" or "c-b-c" simulation.
2) By running ac simulation on the linear circuit in which the rectifier, load and the output capacitance of PZT were replaced by an equivalent R_{eq}, C_{eq} network according to proposed modeling method (Fig. 7). For this case, the dc output voltage was calculated according to (18).

Simulations were carried out on a virtual PZT similar to the Philips' single layer thickness polarization transverse vibration mode PZT (PXE43-S, RT $35 \times 8 \times 2$ mm) for which the following parameters were assumed [16]: series inductance $L_r = 165$ mH, series capacitance $C_r = 15.1$ pF (hence, series resonant frequency $f_r = 100.83$ kHz), output capacitance $C_o = 510$ pF, loss resistance $R_m = 105\ \Omega$ and mechanical transfer ratio $n = 1$.

The simulation results are presented in Tables I and II and Figs. 9 and 10.

Table I summarizes the results for the cases when the load resistance R_L was changed over a wide range and the operating frequency f was corrected so as to get the maximum load voltage $V_{L\,max}$. This Table includes:

— the load resistance R_L and corresponding values of the equivalent resistance R_{eq} and the equivalent capacitance C_{eq};
— the maximum output-to-input ac voltage ratio $(k_{21})_{max}$, and corresponding values of the absolute and normalized frequency $f_{m.mod.ac}$, $\omega^*_{m.mod.ac}$ obtained by simulation of the ac model (Fig. 7);

TABLE II
INFLUENCE OF OPERATING FREQUENCY f ON THE NORMALIZED LOAD VOLTAGE V^*_L. SIMULATION RESULTS. LOAD RESISTANCE $R_L = 10$ kOhm. SUBSCRIPT $_{mod.ac}$ DENOTES SIMULATION RESULTS OF THE AC MODEL (FIG. 7). SUBSCRIPT $_{c-b-c}$ DENOTES RESULTS OF CYCLE-BY-CYCLE SIMULATION OF THE AC/DC CIRCUIT (FIG. 8)

f	$\omega^{**} = \omega/\omega_m$	$V^*_{L\,mod.ac}$	$V^*_{L\,c-b-c}$
Hz	-	-	-
99500	0.98243	0.553	0.555
100000	0.98737	0.745	0.740
100500	0.99231	1.117	1.119
101000	0.99724	1.839	1.843
101279	1	2.130	2.114
101500	1.00218	1.932	1.909
102000	1.00712	1.174	1.162
102500	1.01206	0.775	0.769
103000	1.017	0.568	0.546

— the normalized maximum load voltage $V^*_{L\,max.mod.ac}$ calculated using the results of simulation of the ac model (Fig. 7):

$$V^*_{L\,max.mod.ac} = (k_{21})_{max}\sqrt{\frac{R_{eq}}{2R_L}} \tag{35}$$

— the normalized maximum load voltage $V^*_{L\,max.c-b-c}$ and corresponding frequency $\omega^*_{m.c-b-c}$ obtained by cycle-by-cycle simulation of the ac/dc model (Fig. 8).

Table I also includes the calculation values, according to the equation developed in this study, of the normalized maximum load voltage $V^*_{L\,max.anal}$ and the corresponding frequency $\omega^*_{m.anal}$.

Comparison of $V^*_{L\,max.mod.ac}$, $V^*_{L\,max.c-b-c}$ and $V^*_{L\,max.anal}$ for the same values of the load resistance R_L (Table I) shows that they are practically identical. The frequencies $\omega^*_{m.mod.ac}$, $\omega^*_{m.c-b-c}$ and $\omega^*_{m.anal}$ also coincide. The dependences $V^*_{L\,max}$ and ω^*_m on R_L (Table I) are plotted in Fig. 9(a) and (b). As one can judge, the agreement is very good.

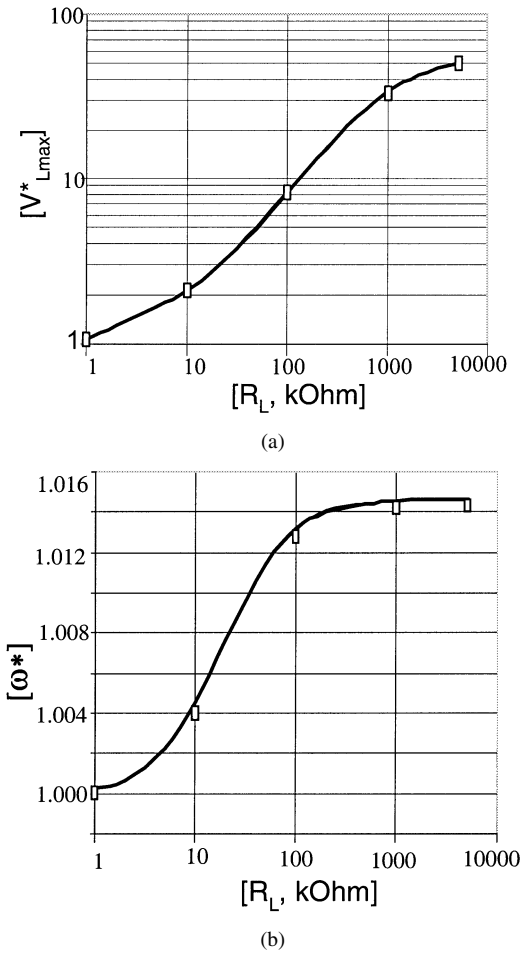

Fig. 9. Normalized maximum load voltage $\mathrm{V}^*_{\mathrm{L\,max}}$ (a) and the corresponding normalized operating frequency ω^* (b) as a function of the load resistance $\mathrm{R_L}$. Solid lines—simulation (ac model) and analytical results; □—results of cycle-by-cycle simulation.

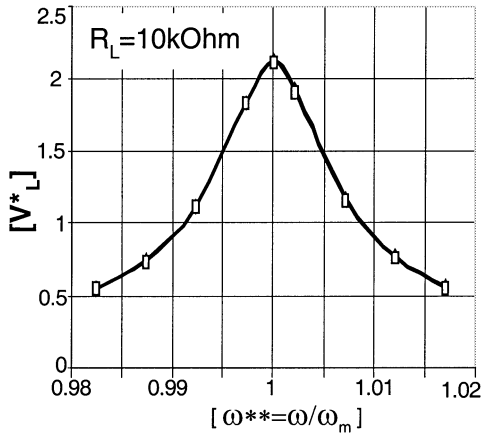

Fig. 10. Influence of operating frequency ω on the normalized load voltage $\mathrm{V}^*_{\mathrm{L}}$. Solid line—ac model simulation, □—cycle-by-cycle simulation. Load resistance $\mathrm{R_L} = 10\ \mathrm{kOhm}$. ω_{m}—operating frequency corresponding to the maximum load voltage $\mathrm{V}^*_{\mathrm{L\,max}}$.

Table II summarizes the results for the cases when the load resistance $\mathrm{R_L}$ is constant (10 kΩ) and the operating frequency f is changed in a narrow range near $\mathrm{f_m}$. This Table includes the values of the normalized dc output voltage obtained by simulation of the ac model (Fig. 7) $\mathrm{V}^*_{\mathrm{L.mod.ac}}$ and by cycle-by-cycle

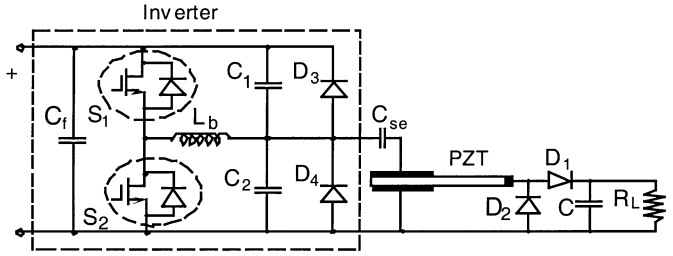

Fig. 11. Experimental circuit.

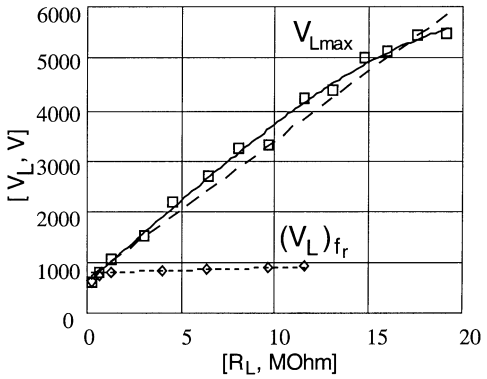

Fig. 12. Load voltage as a function of the load resistance $\mathrm{R_L}$. Experimental data (points) and theoretical model (broken lines). $(\mathrm{V_L})_{\mathrm{f_r}}$—voltage corresponding to the resonant frequency $\mathrm{f_r}$; $\mathrm{V_{Lmax}}$—maximum output voltage reached by frequency adjustment.

simulation of the ac/dc model (Fig. 8) $\mathrm{V}^*_{\mathrm{L.c-b-c}}$. Both values of $\mathrm{V}^*_{\mathrm{L}}$ are practically identical for any given frequency over the tested frequency range. The dependence $\mathrm{V}^*_{\mathrm{L}}$ on $\omega^{**} = \omega/\omega_{\mathrm{m}}$ (Table II) is plotted in Fig. 10.

The experimental set up is shown in Fig. 11. The Philips PZT (PXE43, $48 \times 8 \times 2$ mm, single layer, Rosen type) was fed through a coupling capacitor $\mathrm{C_{se}} = 1\ \mu\mathrm{F}, 630$ V from the output of a half-bridge high frequency inverter driven by a 50% duty cycle. The coupling capacitor was used to block the dc from PZT input electrodes in order to reduce the possibility of depolarization. The inverter included following elements (Fig. 11): $\mathrm{S_1}$ and $\mathrm{S_2}$—transistors IRF740, diodes $\mathrm{D_3}$ and $\mathrm{D_4}$—MUR405, inductor $\mathrm{L_b} = 170\mu\mathrm{H}$ and capacitors $\mathrm{C_1} = \mathrm{C_2} = 3$ nF. The purpose of the LC filter was to soften the squarewave waveform coming out of the half bridge inverter while the diodes were used to clamp the peak voltages to the supply and ground potentials. The output rectifier included high voltage diodes $\mathrm{D_1}$ and $\mathrm{D_2}$—BY187/01 (10 kV, 2 mA). The parameters of the PZT (Fig. 2) as provided by the manufacturer were

$$\mathrm{C_{in}} = 735\ \mathrm{pF}, \mathrm{C_o} = 5.5\ \mathrm{pF}, \mathrm{C_r} = 24.5\ \mathrm{pF},$$
$$\mathrm{L_r} = 201\ \mathrm{mH}, \mathrm{R_m} = 63\,\Omega \text{ and } \mathrm{n} = 5.6.$$

The validity of these parameters was verified by comparing simulation results that were run on the PZT model with these values to experimental measurements taken by a network analyzer (HP4395A).

The frequency range was 65–80 kHz. The load resistance $\mathrm{R_L}$ was changed from 395 kΩ to 19.2 MΩ. Relationships between the load voltage $\mathrm{V_L}$ and $\mathrm{R_L}$ were measured in two cases (Fig. 12):

1) when the operating frequency f was equal to the resonant frequency f_r. For the PZT under study, $f_r = 71.72$ kHz;
2) when f was corrected so as to get maximum output voltage: $V_L = V_{Lmax}$.

The rms input voltage of PZT $V_{in\ rms}$ was held constant: 62 V in the first case and 52.5 V in the second case.

The deviation of the model prediction from the experimental results (Fig. 12) was found to be smaller than 13%.

VI. Discussion

The presented approach can be considered as a modification of the approximate analysis of steady state processes in voltage-fed parallel and series-parallel resonant converters with capacitive output filter [15]. The new approach presented in this paper is simpler since capacitance C_o is included in the $R_{eq}C_{eq}$ equivalent circuit; so it is unnecessary now to obtain the phase angle between the first harmonics of the capacitor's C_o voltage and the input current of the rectifier. Additional capacitance C_{ad} obtained from (22) is equivalent to the value C_e given in [15].

The system under study is of a high order and consequently, precise analytical relationships are difficult if not impossible to derive. The proposed approximate derivation is based on the assumption that the numerical value of (C_r/n^2C_o) is small. It was found that this assumption is valid for practical PZT devices because one finds that when n is large C_o is normally small. For the PZTs tested in this study we find that the value of (C_r/n^2C_O) was about 0.1 for the Rosen type PZT and 0.029 for the PZT model used in the simulation studies. When (C_r/n^2C_O) is small, the expected range for $(\omega/\omega_r)_{max}$ per (29) is small. For such a narrow frequency window, $\varphi_{(1)}$ and C_{eq} can be assumed to be approximately constant (Fig. 4 and 6) which makes possible taking the approximate derivative of (24) to find $(\omega/\omega_r)_{max}$. If the frequency window for $(\omega/\omega_r)_{max}$ of a given PZT is not narrow, the approximate equations derived here may not apply.

The extensive simulation tests of the proposed modeling and analysis approach as well as the experimental measurements suggest that the approximate analysis developed here is accurate for a wide range of PZT elements. It should be noted that the simulation verification was done for a symmetrical device $(n = 1)$ with a relative large output capacitor whereas the experiments were run on a Rosen type of $n = 5.6$ and relatively small output capacitor. The modeling approach was found to be accurate for these very different devices, suggesting that the method could be useful for a variety of PZT families.

The analysis presented above was carried out for the voltage doubler rectifier which is a private case of the capacitive filter rectifier family. The analytical results can be easily translated to other rectifiers with a capacitive filter. Consider for example the full bridge capacitive loaded rectifier. The comparison is carried out under the condition that the rectifiers are fed by PZTs with identical parameters, both rectifiers operate at the same frequency ω, process the same power with the same diodes conduction angle θ and hence with identical voltage waveform across the output capacitance C_o of the PZTs. Since the output voltage of the voltage doubler rectifier $V_{L.D}$ is equal to this peak-to-peak voltage of the capacitor, while the output voltage of the full bridge rectifier $V_{L.Br}$ is twice lower, we find

$$V_{L.Br} = 0.5\ V_{L.D}. \tag{36}$$

For equal power

$$\frac{V_{L.Br}^2}{R_{L.Br}} = \frac{V_{L.D}^2}{R_{L.D}} \tag{37}$$

and therefore the ratio of load resistances of the two rectifiers will be

$$\frac{R_{L.Br}}{R_{L.D}} = 0.25. \tag{38}$$

VII. Conclusion

The results cycle-by-cycle and ac simulations verify the accuracy of the proposed ac model. It is clear from these results that the RC equivalent model can replace the rectifier-load section in symbolic and numeric analytical derivations and in circuit simulation. Hence, when applicable, the proposed $R_{eq}C_{eq}$ model offers a simple way to analyze and simulate the behavior of the ac–dc HV PZT circuit. Furthermore, since the resulting equivalent circuit is SPICE compatible it can be used to examine by simulation the behavior of the PZT-rectifier assembly by running frequency domain (ac) analysis, which is much faster than cycle-by-cycle time domain simulation (TRAN).

References

[1] C. Y. Lin and F. C. Lee, "Development of a piezoelectric transformer converter," in *Proc. VPEC Sem.*, Blacksburg, VA, 1993, pp. 79–85.
[2] Philips Components, "Piezoelectric transformers," Application Note, Philips Magnetic Products, Feb. 1997.
[3] M. Shoyama, K. Horikoshi, T. Ninomiya, T. Zaitsu, and Y. Sasaki, "Operation analysis of the push-pull piezoelectric inverter," in *Proc. IEEE APEC'97*, 1997, pp. 573–578.
[4] ——, "Steady-state characteristics of the push-pull piezoelectric inverter," in *Proc. IEEE PESC'97 Conf.*, 1997, pp. 715–721.
[5] H. Kakehashi, T. Hidaka, T. Ninomiya, M. Shoyama, H. Ogasawara, and Y. Ohta, "Electronic ballast using piezoelectric transformers for fluorescent lamps," in *Proc. IEEE PESC'98 Conf.*, 1998, pp. 29–35.
[6] T. Yamane, S. Hamamura, T. Zaitsu, T. Ninomiya, M. Shoyama, and Y. Fuda, "Efficiency improvement of piezoelectric-transformer dc-dc converter," in *Proc. IEEE PESC'98 Conf.*, 1998, pp. 1255–1261.
[7] A. M. Flynn and S. R. Sanders, "Fundamental limits on energy transfer and circuit considerations for piezoelectric transformers," in *Proc. IEEE PESC'98 Conf.*, 1998, pp. 1463–1471.
[8] S. Ben-Yaakov, M. Shvartsas, and G. Ivensky, "A piezoelectric cold cathode fluorescent lamp driver operating from a 5 Volt bus," in *Proc. PCIM'00*, Nürnberg, Germany, 2000, pp. 379–383.
[9] J. Navas, T. Bove, J. A. Cobos, F. Nuño, and K. Brebol, "Miniaturised battery charger using piezoelectric transformers," in *Proc. IEEE APEC'01*, 2001, pp. 492–496.
[10] M. J. Prieto, J. Diaz, J. A. Martin, and F. Nuño, "A very simple dc/dc converter using piezoelectric transformer," in *Proc. IEEE PESC'01 Conf.*, 2001, pp. 1755–1760.
[11] E. Dallago, A. Danioni, M. Passoni, and G. Venchi, "Modeling of dc-dc converter based on a piezoelectric transformer and its control loop," in *Proc. IEEE PESC'02 Conf.*, 2002, pp. 927–931.
[12] M. Sanz, P. Alou, A. Soto, R. Prieto, J. A. Cobos, and J. Uceda, "Magnetic-less converter based on piezoelectric transformers for step-down dc/dc and low power application," in *Proc. IEEE APEC'03 Conf.*, 2003, pp. 657–662.

[13] S. Ben-Yaakov and S. Lineykin, "Frequency tracking to maximum power of piezoelectric transformer HV converter under load variations," in *Proc. IEEE PESC'02 Conf.*, 2002, pp. 657–662.
[14] G. Ivensky, I. Zafrany, and S. Ben-Yaakov, "Generic operational characteristics of piezoelectric transformers," *IEEE Trans. Power Electron.*, vol. 17, pp. 1049–1057, Nov. 2002.
[15] G. Ivensky, A. Kats, and S. Ben-Yaakov, "A RC load model of parallel and series-parallel resonant dc-dc converters with capacitive output filter," *IEEE Trans. Power Electron.*, vol. 14, pp. 958–964, May 1999.
[16] G. Ivensky, S. Bronstein, and S. Ben-Yaakov, "Analysis and design of a piezoelectric transformer ac/dc converter in a low voltage application," in *Proc. IEEE PESC'02 Conf.*, 2002, pp. 409–414.

Gregory Ivensky was born in Leningrad, Russia, in 1927. He received the B.S. degree in energy engineering from the Leningrad Railway Transport Institute, Leningrad, Russia, in 1948 and the M.S. and Ph.D. degrees from the Leningrad Polytechnic Institute, Leningrad, in 1958 and 1977, respectively.

From 1951 to 1962, he was with the Central Design Bureau of Ultrasound and High Frequency Devices, Leningrad. From 1962 to 1989, he was at the North-Western Polytechnic Institute, Leningrad, where in 1980 he became a Full Professor in the Department of Electronic Devices. Since 1991, he has been a Professor at the Department of Electrical and Computer Engineering, Ben-Gurion University of the Negev, Beer-Sheva, Israel. His research interests include rectifiers, inverters, dc–dc converters, EMI and power quality issues, and induction heating.

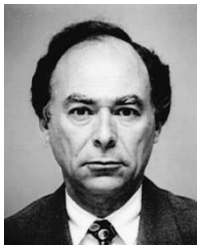

Moshe Shvartsas was born in Vilnius, Lithuania, in 1946. He received the M.S. degree in physics from Vilnius State University, Lithuania, in 1967 and the Ph.D. degree from the St. Petersburg Institute of Labor Protection, St. Petersburg, Russia.

From 1967 to 1993, he was with the R&D Institute of Electrical Welding Equipment, Vilnius, as a Researcher. He has specialized in welding generators, motor-generators, and welding electrical arc noise reduction. Since 1996, he has been a co-worker at the Department of Electrical and Computer Engineering, Ben-Gurion University of the Negev, Beer-Sheva, Israel. His current interests include electrical arc, power supplies, and SPICE modeling.

Shmuel (Sam) Ben-Yaakov (M'87) was born in Tel Aviv, Israel, in 1939.gree in electrical engineering from the Technion, Haifa, Israel, in 1961 and the M.S. and Ph.D. degrees in engineering from the University of California, Los Angeles, in 1967 and 1970, respectively.

He is presently a Professor with the Department of Electrical and Computer Engineering, Ben-Gurion University of the Negev, Beer-Sheva, Israel, where he heads the Power Electronics Group. He served as the Chairman of that department from 1985 to 1989. His current research interests include power electronics, circuits and systems, electronic instrumentation, and engineering education. He also serves as Chief Scientist of Green Power Technologies Ltd, Israel, and as a consultant to commercial companies on various subjects, including analog circuit design and power electronics.